

# Tuning Photophysics and Nonlinear Absorption of Bipyridyl Platinum(II) Bisstilbenylacetylide Complexes by Auxiliary Substituents

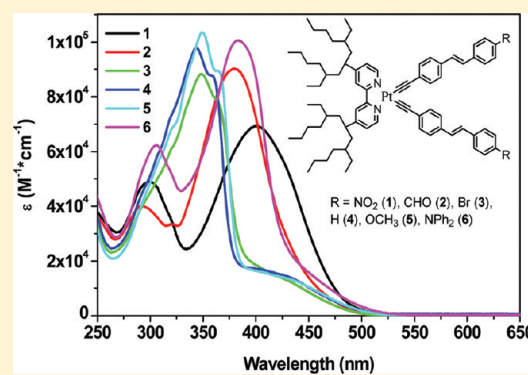
Zhongjing Li,<sup>†</sup> Ekaterina Badaeva,<sup>†</sup> Dapeng Zhou,<sup>‡</sup> Josiah Bjorgaard,<sup>†</sup> Ksenija D. Glusac,<sup>‡</sup> Svetlana Killina,<sup>†</sup> and Wenfang Sun<sup>\*,†</sup>

<sup>†</sup>Department of Chemistry and Biochemistry, North Dakota State University, Fargo, North Dakota 58108-6050, United States

<sup>‡</sup>Department of Chemistry, Bowling Green State University, Bowling Green, Ohio 43403-0001, United States

## S Supporting Information

**ABSTRACT:** The photophysics of six bipyridyl platinum(II) bisstilbenylacetylide complexes with different auxiliary substituents are reported. These photophysical properties have been investigated in detail by UV-vis, photoluminescence (both at room temperature and at 77 K) and transient absorption (nanosecond and femtosecond) spectroscopies, as well as by linear response time-dependent density functional theory (TD-DFT) calculations. The photophysics of the complexes are found to be dominated by the singlet and triplet  $\pi,\pi^*$  transitions localized at the stilbenylacetylide ligands with strong admixture of the metal-to-ligand (MLCT) and ligand-to-ligand (LLCT) charge-transfer characters. The interplay between the  $\pi,\pi^*$  and MLCT/LLCT states depends on the electron-withdrawing or -donating properties of the substituents on the stilbenylacetylide ligands. All complexes exhibit remarkable reverse saturable absorption (RSA) at 532 nm for nanosecond laser pulses, with the complex that contains the NPh<sub>2</sub> substituent giving the strongest RSA and the complex with NO<sub>2</sub> substituent showing the weakest RSA.



## INTRODUCTION

Photophysical and photochemical properties of platinum complexes have been of intense interest for researchers for several decades. These interests arise from the unique structural and spectroscopic properties of the platinum complexes and their promising potential applications in the fields of organic light-emitting diodes (OLEDs),<sup>1</sup> low power photon upconversion sensitizers,<sup>2</sup> dye-sensitized solar cells (DSSCs),<sup>3</sup> DNA intercalators,<sup>4</sup> photodynamic therapy (PDT),<sup>5</sup> and so forth. Among the reported complexes, platinum diimine bis(acetylide) complexes are of particular interest. Systematic investigations of the photophysics and potential applications of these complexes have been reported by several groups. In 1994, Che and co-workers reported their study on the Pt(phen)(C≡CC<sub>6</sub>H<sub>5</sub>)<sub>2</sub> complexes and proposed that the emissive state for these complexes has a metal-to-ligand charge-transfer character (MLCT).<sup>6,7</sup> Following that, comprehensive work by Eisenberg's group discovered that the lowest occupied molecular orbital (LUMO) of the Pt(II) diimine complexes could be adjusted by variation of the substituents on diimine, while the highest occupied molecular orbital (HOMO) was slightly affected by the variation of the arylacetylide ligands.<sup>8</sup> Schanze and co-workers later reported that the intraligand  $^3\pi,\pi^*$  state largely localized on the arylacetylide ligand could also play a role in the photophysics of the Pt(II) diimine complex with strong electron-withdrawing group on the phenylacetylide ligands.<sup>9</sup> In recent

years, Castellano and co-workers demonstrated the interplay of the  $^3\text{MLCT}$  and  $^3\pi,\pi^*$  states in Pt(II) diimine complexes bearing more conjugated aromatic rings, that is, 1-pyrene, 1-anthracene, and 1-perylene on the acetylide ligands.<sup>10</sup> In accordance with these results, our group recently revealed the admixture of the  $^3\text{MLCT}$  and  $^3\pi,\pi^*$  characters in the lowest excited states of a 2,2'-bipyridine Pt(II) complex bearing 2-(benzothiazol-2'-yl)-9,9-diethyl-7-ethynylfluorene ligands.<sup>11</sup>

In addition to the interesting photophysical studies, the potential applications of the Pt(II) diimine complexes in OLEDs,<sup>12</sup> molecular photochemical devices,<sup>13</sup> and as vapoluminescent materials<sup>14</sup> and nonlinear absorbing materials<sup>11</sup> have been explored. A detailed nonlinear absorption study reported by our group on the 2,2'-bipyridine Pt(II) complex bearing 2-(benzothiazol-2'-yl)-9,9-diethyl-7-ethynylfluorene ligands<sup>11</sup> revealed that this complex exhibited extremely large ratios of the excited-state absorption relative to that of the ground state in the visible spectral region and large two-photon absorption (TPA) in the near-IR region. This discovery is quite exciting; however, the two-photon absorption cross sections of this complex are still moderate compared to those of the best organic two-photon absorbing materials.<sup>15</sup> In order to improve

Received: March 6, 2012

Revised: April 11, 2012

Published: April 21, 2012

**Scheme 1: Synthesis of Pt(II) complexes 21-26**

The scheme illustrates the synthesis of Pt(II) complexes 21-26 from Pt(IV) complex 20. The Pt(IV) complex 20 is a dicationic complex with two terphenyl ligands and two terphenyl-ethynyl ligands. It is converted to Pt(II) complex 22 using  $K_2PtCl_4$  and dilute HCl aq. refluxing. Complex 22 is then converted to Pt(II) complexes 21-26 using  $CuI$ , DCM/DIA, and 2 eq. of the corresponding terphenyl-ethynyl ligand (1-6). The ligands are: 1 (R = NO<sub>2</sub>), 2 (R = CHO), 3 (R = Br), 4 (R = H), 5 (R = OCH<sub>3</sub>), 6 (R = NPh<sub>2</sub>).

**Reaction 1: Synthesis of 21-26 from 20**

20 + 2 eq. of ligand (1-6)  $\xrightarrow{Cul, DCM/DIA, \text{Reflux under argon for 24 hrs}}$  21-26 (20% ~ 60% yield)

**Reaction 2: Synthesis of 22 from 20**

20  $\xrightarrow{K_2PtCl_4, \text{Dilute HCl aq., refluxing}}$  22

**Reaction 3: Synthesis of 19 from 18**

18 + Ph<sub>2</sub>NH, 18-crown-6, Cu, K<sub>2</sub>CO<sub>3</sub>, mesitylene  $\xrightarrow{\text{Reflux, Ar, 9 hrs}}$  19 (70% yield)

**Reaction 4: Synthesis of 20 from 19**

19 + (Triethylsilyl)acetylene, Cul, Ph<sub>3</sub>P, Pd(PPh<sub>3</sub>)<sub>2</sub>Cl<sub>2</sub>, Et<sub>3</sub>N/THF  $\xrightarrow{\text{Reflux, 24 hrs}}$  20 (37% yield)

**Reaction 5: Synthesis of 18 from 17**

17 + 4-Bromobenzaldehyde, NaH, THF  $\xrightarrow{\text{Reflux, 24 hrs}}$  18 (29% yield)

**Reaction 6: Synthesis of 17 from 1**

1 + PO(OEt)<sub>3</sub>  $\xrightarrow{160^\circ C, 10 \text{ hrs}}$  17 (57% yield)

**Reaction 7: Synthesis of 16 from 15**

15 + Cul, Pd(PPh<sub>3</sub>)<sub>4</sub>, PPh<sub>3</sub>, Et<sub>3</sub>N  $\xrightarrow{\text{Reflux, Ar, 8 hrs}}$  16 (80% yield)

**Reaction 8: Synthesis of 15 from 13**

13 + 4-Methoxystyrene, [Pd(OAc)<sub>2</sub>]<sub>3</sub>, MeCN/Et<sub>3</sub>N  $\xrightarrow{\text{Reflux, 12 hrs, Ar}}$  15 (52% yield)

**Reaction 9: Synthesis of 14 from 13**

13 + Pd(PPh<sub>3</sub>)<sub>4</sub>, Cul, Ph<sub>3</sub>P, Et<sub>3</sub>N/THF  $\xrightarrow{\text{Reflux, Ar, 12 hrs}}$  14 (82% yield)

**Reaction 10: Synthesis of 13 from 11**

11 + Styrene, Pd(OAc)<sub>2</sub>, Et<sub>3</sub>N/MeCN  $\xrightarrow{\text{Reflux, 12 hrs}}$  13 (77% yield)

**Reaction 11: Synthesis of 10 from 9**

9 + Pd(PPh<sub>3</sub>)<sub>4</sub>, Cul, Ph<sub>3</sub>P, Et<sub>3</sub>N  $\xrightarrow{\text{Reflux, Ar, 20 hrs}}$  10 (70% yield)

**Reaction 12: Synthesis of 9 from 7**

7 + 4-bromostyrene, Pd(Ph<sub>3</sub>P)<sub>2</sub>Cl<sub>2</sub>, Et<sub>3</sub>N/DMF  $\xrightarrow{120^\circ C, Ar, 16 \text{ hrs}}$  9 (33% yield)

**Reaction 13: Synthesis of 8 from 7**

7 + Cul, Pd(PPh<sub>3</sub>)<sub>4</sub>, PPh<sub>3</sub>, Et<sub>3</sub>N  $\xrightarrow{\text{Reflux, Ar, 12 hrs}}$  8 (68% NO<sub>2</sub>, 36% Br)

**Reaction 14: Synthesis of 1 from 8**

8 + KOH, i-PrOH  $\xrightarrow{\text{Reflux, Ar, 3 hrs}}$  1-L (15% NO<sub>2</sub>, 46% Br)

**Reaction 15: Synthesis of 2 from 8**

8 + K<sub>2</sub>CO<sub>3</sub>, CH<sub>2</sub>Cl<sub>2</sub>/MeOH  $\xrightarrow{\text{Reflux, Ar, 3 hrs}}$  2-L (67% yield)

**Reaction 16: Synthesis of 4-L from 14**

14 + KOH, 2-propanol  $\xrightarrow{\text{Reflux, Ar, 3 hrs}}$  4-L (80% yield)

**Reaction 17: Synthesis of 5-L from 16**

16 + KOH, i-PrOH  $\xrightarrow{\text{Reflux, Ar, 3 hrs}}$  5-L (80% yield)

In this study, we synthesized a series of platinum diimine bisstilbenylacetylide complexes with different substituents on the stilbene motif (Scheme 1, complexes **1–6**) and systematically investigated their photophysics and excited-state absorption. The nonlinear transmission performances of these complexes were evaluated at 532 nm using nanosecond laser pulses. Although the ultimate goal of this project is to enhance the TPA of the Pt(II) complexes in the near-IR region, the linear optical properties of these complexes and their dependence on the substituents are in close relationship to the nonlinear absorption of the complexes. As such, we first focus on understanding how the

auxiliary substituents on the stilbenylacetylide ligand influence the ground-state and excited-state characteristics of the complexes. To reach this goal, both photophysical experiments and time-dependent density functional theory (TD-DFT) calculations were carried out. To the best of our knowledge, it is the first time that such an effect has been explored for Pt(II) complexes bearing substituted stilbenylacetylide ligands. It is also the first time that the excited-state absorption and nonlinear transmission of the Pt(II) bisstilbenylacetylide complexes is systematically investigated.

## ■ EXPERIMENTAL SECTION

**Synthesis and Characterization.** All of the reagents and solvents for synthesis were purchased from Aldrich Chemical Co. or Alfa Aesar and used as received, unless otherwise stated. Silica gel for chromatography was purchased from Sorbent Technology (60 Å, 230–400 mesh, 500–600 m<sup>2</sup>/g, pH: 6.5–7.5). Complexes 1–6 were characterized by <sup>1</sup>H NMR, electrospray ionization mass spectrometry (ESI-MS), and elemental analyses. Ligands 3-L–6-L were characterized by <sup>1</sup>H NMR and elemental analyses. Each intermediate was characterized by <sup>1</sup>H NMR. <sup>1</sup>H NMR was obtained on Varian Oxford-VNMR spectrometers (300, 400, or 500 MHz). ESI-MS analyses were performed at a Bruker BioTOF III mass spectrometer. Elemental analyses were conducted by NuMega Resonance Laboratories, Inc. in San Diego, California.

4,4'-Di(5,9-diethyltridecan-7-yl)-2,2'-bipyridine (**21**) was synthesized following the literature procedure.<sup>18</sup> Complex **22** was synthesized by the reaction of K<sub>2</sub>PtCl<sub>4</sub> with **21** in refluxing aqueous HCl solution.<sup>8</sup> Compounds **7**, **9**, **11**, **13**, and **15** were synthesized by the Heck reaction.<sup>19</sup> Compound **18** was synthesized by the Wittig reaction.<sup>20</sup> Compound **19** was synthesized by the Ullmann reaction<sup>21</sup> from **18**. The Sonogashira coupling reaction<sup>22</sup> of **7**, **9**, **11**, **13**, **15**, and **19** with ethynyltrimethylsilane or 2-methyl-3-butyne-2-ol followed by hydrolysis with K<sub>2</sub>CO<sub>3</sub> or KOH in *i*-PrOH afforded ligands **1-L–6-L**. The synthesis of **1-L–6-L** was all previously reported,<sup>17,23</sup> except for **3-L**, whose synthesis is described in the Supporting Information. The <sup>1</sup>H NMR data for compounds **21** and **22** are also provided in the Supporting Information. The target complexes **1–6** were obtained by reaction of complex **22** with the respective stilbenylacetylide ligand using diisopropylamine as the base and CuI as the catalyst. The synthetic procedure and characterization data for **1–6** are provided in the Supporting Information.

**DFT Calculations.** The ground- and excited-state properties of complexes **1–6** were studied using DFT and linear response TD-DFT. All calculations (ground-state geometry optimization, electronic structure, excited states, and optical spectra) were performed using the Gaussian 09 quantum chemistry software package.<sup>24</sup> The geometries of all molecules were optimized for the ground state (closed-shell singlet S<sub>0</sub>). For calculations of emission spectra, the geometry was optimized in the lowest-energy excited singlet (S<sub>1</sub>) and triplet (T<sub>1</sub>) states. All procedures were done utilizing the hybrid long-range corrected CAM-B3LYP functional.<sup>25</sup> The LANL08 basis set was used for the heavier Pt atom, while the remaining atoms were modeled with the 6-31G\* basis set. The chosen method represents one of the currently most accurate DFT functionals and basis sets that have already shown good agreement with experimental data for different organometallic complexes.<sup>26</sup> All calculations have been performed in solvent using the CPCM reaction field model,<sup>27</sup> as implemented in Gaussian 09. Dichloromethane

(CH<sub>2</sub>Cl<sub>2</sub>, ε<sub>r</sub> = 8.93) was chosen as a solvent for consistency with the experimental studies. As was found for several organometallic complexes, inclusion of the solvent into calculations is very important to reproduce experimental optical spectra.<sup>28</sup>

For computations of emission energies, the excited-state geometry optimization has been performed with analytic TD-DFT gradients<sup>29,30</sup> using the long-range corrected functional CAM-B3LYP. For the absorption spectra of the complexes, the 40 lowest singlet optical transitions were considered to reach the transition energies of ~4.9 eV. Each spectral line obtained from the TD-DFT calculation was broadened by a Gaussian function with the line width of 0.1 eV to match the experimentally observed homogeneous broadening. The fluorescence energies were determined by calculating vertical transition energies for the optimized lowest singlet excited state (S<sub>1</sub>) geometries (both excited-state geometry optimization and vertical transitions have been performed with the TD-DFT). The phosphorescence energies were calculated by first optimizing the lowest triplet-state geometry followed by the vertical triplet excitations calculated via TD-DFT.

In order to analyze the nature of the singlet and triplet excited states, natural transition orbital (NTO) analysis was performed.<sup>31</sup> NTOs are obtained via separate unitary transformations applied to the occupied (hole) and the unoccupied (electron) orbitals. Such unitary transformation diagonalizes the transition density matrix obtained from TD-DFT calculations and gives the best representation of the electron excitation in single-particle terms. In other words, this method offers the most compact representation of the transition density as a single pair of an electron–hole excitation from the ground state. Here, we refer to the unoccupied NTO (to which an electron is excited) as the “electron” transition orbital and the occupied NTO (from which an electron was transferred) as the “hole” transition orbital. Note that electron and hole NTOs are not the same as unoccupied and occupied molecular orbitals (MOs) in their ground state. Upon photoexcitation, the excitonic couplings (Coulomb interaction between the photoexcited electron–hole pair) mix the ground state MOs, so that the representation of an excitation via the pair of ground-state MOs is not valid. In contrast, electron and hole NTOs obtained from TD-DFT calculations allow for representation of the excited-state electronic density. NTOs shown in this paper were produced with the isovalue of 0.02 and visualized with the GaussView 5.1 graphical software.<sup>32</sup>

**Photophysical Measurements.** The solvents used for photophysical experiments were spectroscopic grade, which were purchased from VWR International and used as received without further purification. An Agilent 8453 spectrophotometer was used to record the UV–vis absorption spectra in different solvents. A SPEX fluorolog-3 fluorometer/phosphorometer was used to record the steady-state emission spectra in different solvents. The emission quantum yields were determined by the relative actinometry method<sup>33</sup> in degassed solutions, in which a degassed 1 N sulfuric acid solution of quinine bisulfate (Φ<sub>em</sub> = 0.546, λ<sub>ex</sub> = 347.5 nm)<sup>34</sup> was used as the reference.

The laser system for the femtosecond transient absorption measurement was described previously.<sup>35</sup> Briefly, the 800 nm laser pulses were produced at a 1 kHz repetition rate (fwhm = 110 fs) by a mode-locked Ti:sapphire laser (Hurricane, Spectra-Physics). The output from the Hurricane was split into pump (85%) and probe (10%) beams. The pump beam (800 nm) was sent into an optical paramagnetic amplifier (OPA-400, Spectra Physics) to obtain 310, 330, and 350 nm excitation sources



( $E < 1 \mu\text{J}/\text{pulse}$ ) and to a second harmonic generator (Super Tripler, CSK) to obtain a 400 nm beam ( $E \approx 2 \mu\text{J}/\text{pulse}$ ). The probe beam was focused into a rotating  $\text{CaF}_2$  crystal or a sapphire crystal for white light continuum generation between 350 and 750 nm or between 400 and 800 nm. The flow cell (Starna Cell Inc. 45-Q-2, 0.9 mL volume with a 2 mm path length), pumped by a Fluid Metering RSHY Lab pump (Scientific Support Inc.), was used to prevent photodegradation of the sample. After passing through the cell, the continuum was coupled into an optical fiber and input into a CCD spectrograph (Ocean Optics, S2000). The data acquisition was achieved using in-house LabVIEW (National Instruments) software routines. The group velocity dispersion of the probing pulse was determined using nonresonant optical Kerr effect (OKE) measurements.<sup>36</sup> Sample solutions were prepared at a concentration needed to have absorbance of  $A \approx 0.6\text{--}0.8$  at the excitation wavelength.

The nanosecond transient absorption (TA) spectra and decays were measured in degassed solutions on an Edinburgh LP920 laser flash photolysis spectrometer. The third harmonic output (355 nm) of a Nd:YAG laser (Quantel Brilliant, pulse width = 4.1 ns, repetition rate set at 1 Hz) was used as the excitation source. Each sample was purged with argon for 30 min before each measurement. The triplet excited-state absorption coefficient ( $\varepsilon_T$ ) at the TA band maximum was determined by the singlet depletion method.<sup>37</sup> The following equation was used to calculate the  $\varepsilon_T$ .<sup>37</sup>

$$\varepsilon_T = \varepsilon_S \frac{\Delta\text{OD}_T}{\Delta\text{OD}_S}$$

where  $\Delta\text{OD}_S$  is the minimum of the bleaching band and  $\Delta\text{OD}_T$  is the maximum of the absorption band in the TA spectrum and  $\varepsilon_S$  is the ground-state molar extinction coefficient at the wavelength of the bleaching band minimum. After the  $\varepsilon_T$  value was obtained, the  $\Phi_T$  could be obtained by the relative actinometry, in which SiNc in benzene was used as the reference ( $\varepsilon_{590} = 70000 \text{ M}^{-1} \text{ cm}^{-1}$ ;  $\Phi_T = 0.20$ ).<sup>38</sup>

**Nonlinear Transmission.** The reverse saturable absorption of complexes 1–6 was characterized by a nonlinear transmission experiment at 532 nm using a Quantel Brilliant laser. The pulse width of the laser was 4.1 ns, and the repetition rate was set at 10 Hz. The complexes were dissolved in  $\text{CH}_2\text{Cl}_2$ . The concentration of the sample solutions was adjusted to obtain a linear transmission of 80% at 532 nm in a 2 mm thick cuvette. The experimental setup and details are similar to those reported previously.<sup>39</sup> A 40 cm plano-convex lens was used to focus the beam to the center of the 2 mm thick sample cuvette.

## RESULTS AND DISCUSSION

**Molecular Geometries.** The optimized geometries of complexes 1–6 are reported in the Supporting Information (Table 1s). Optimization of the ground singlet state of the complexes 1–6 with DFT resulted in their essentially planar geometry. The stilbenyl components of the stilbenylacetylide ligands were twisted relative to the Pt coordination plane by  $\sim 1^\circ$ , while substituent groups stayed in the stilbenyl plane (except for the  $\text{NPh}_2$  group, which was twisted in the propeller-like shape). The average Pt–N bond length was 2.087 Å and was not affected by the stilbenylacetylide substituent group. Pt–C bond lengths were  $\sim 1.940$  Å and were very slightly affected by the substituent groups (in the fourth decimal digit).

**Electronic Absorption.** The UV–vis spectra of complexes 1–6 are shown in Figure 1. The absorption of all complexes

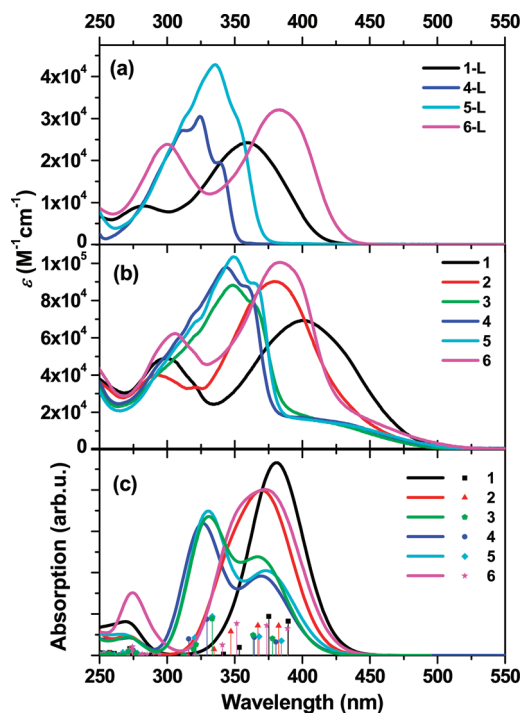


**Figure 1.** (a) UV–vis absorption spectra of ligands 1-L, 4-L, 5-L, and 6-L measured in  $\text{CH}_2\text{Cl}_2$ . (b) UV–vis absorption spectra of complexes 1–6 measured in  $\text{CH}_2\text{Cl}_2$ . (c) Calculated absorption spectra for complexes 1–6; vertical lines resemble excited states and the corresponding oscillator strength.

obeys Lambert–Beer’s law in the concentration range of our study ( $1 \times 10^{-6}$  to  $1 \times 10^{-4}$  mol/L), suggesting that no ground-state aggregation occurs in this concentration range. The major absorption bands of complexes 1–6 (Figure 1b) resemble those of their ligands (shown in Figure 1a), which are exemplified in Figure 1a and b for 1, 4, 5, and 6, indicating that these bands arise from the stilbenylacetylide ligands. This assignment is supported by the molar extinction coefficients of these bands, which are at least double those of their corresponding ligands. The red-shift of these bands suggests delocalization induced by the  $d\pi$  orbital of platinum. The absorption of complexes 3–5 in the region of 300 and 375 nm features well-resolved vibronic structures, which is indicative of the  $^1\pi,\pi^*$  transitions localized on the stilbenylacetylide ligands. However, at the wavelengths above 380 nm, a broad shoulder that is absent in the ligands’ absorption spectra is observed. Compared to the major absorption bands centered at  $\sim 340\text{--}350$  nm, this shoulder exhibits a significant negative solvatochromic effect (as illustrated in Figure 2a), which is consistent with the other Pt(II) diimine complexes reported in the literature<sup>6–9</sup> and implies a charge-transfer nature of this absorption band. In contrast, the absorption spectra of 1, 2, and 6 are broad and red-shifted relative to the major absorption bands of 3–5. The vibronic structures are not clearly observed for 1, 2, and 6. Absorption of complexes 1 and 6 were also found to exhibit a negative solvatochromic effect, as illustrated in Figure 2c for 1. All of these features lead to the attribution of the absorption of 1, 2, and 6 partially to charge-transfer processes, probably mixing ligand-to-ligand charge transfer

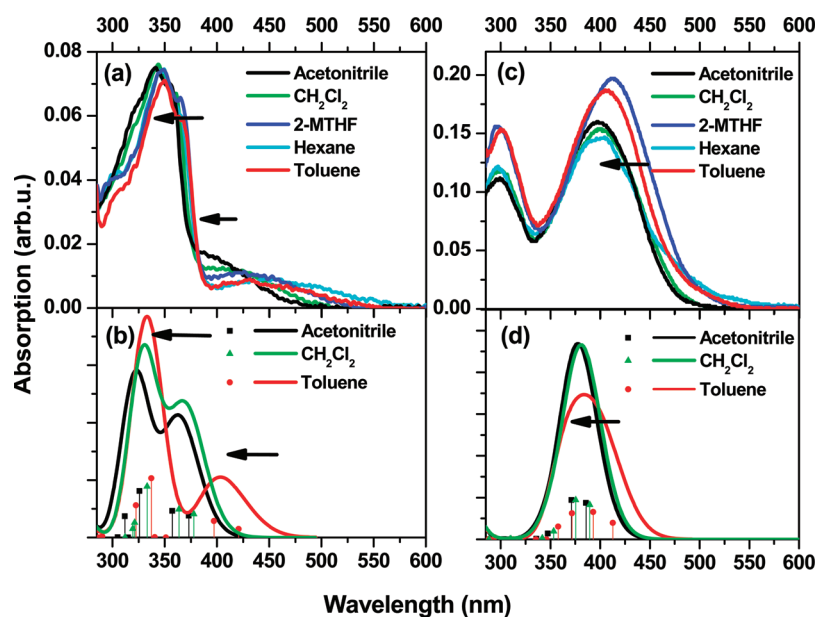


**Figure 2.** (a) Experimental and (b) calculated absorption spectra of complex **4** in different solvents. (c) Experimental and (d) calculated absorption spectra of **1** in different solvents. Arrows indicate the blue shift of the absorption bands with increasing solvent polarity. In panels (b) and (d), the vertical lines resemble excited states and the corresponding oscillator strength.

(LLCT) and MLCT from  $d\pi$  (platinum) to  $\pi^*$  (diimine). However, considering the large molar extinction coefficients of **1**, **2**, and **6**, the lowest-energy absorption band in these three complexes should have dominant contribution from the acetylide ligand  $\pi, \pi^*$  transition.

In general, the major absorption bands of all substituted stilbenylacetylide complexes are red-shifted relative to that of complex **4**, and a similar pattern is observed in the ligands' absorption. This result agrees with the previous study of the push–pull conjugated oligomers<sup>40</sup> and suggests that electronic structures of the Pt complexes discussed in this work can be effectively tuned by varying the substituents at the 4'-position of the stilbenylacetylide ligands, which consequently influences the photophysical properties.

These trends, as well as the overall spectral assignment are supported by the linear response TD-DFT calculations. Calculated absorption spectra (Figure 1c) show a substantial agreement with the experimental data, as can be seen in Figures 1 and 2. Although theoretically predicted absorption energies (Figure 1c) are blue-shifted compared to experimental ones, they clearly reproduce the experimental trends of absorption spectra and are found to be highly dependent on solvent polarity (Figure 2b). Experimental and theoretical absorption properties are summarized and compared in Table 1. Unlike **1**, **2**, and **6**, complexes **3–5**, which are substituted with weak electron–donor/acceptor groups, exhibit a lower-intensity shoulder in the spectral region above 380 nm. As resolved by the DFT studies, the shoulder involves two excitations with mixed MLCT and LLCT character, while the higher-energy peak has dominant ligand  $\pi, \pi^*$  character.

The excited-state character of the studied complexes can be easily seen from the NTO plots, which represent the optical transition as a single pair of the excited electron and the empty hole orbitals as a result of an electron photoexcitation from the ground state. NTOs are shown in Table 2 and in the Supporting Information. Thus, the lowest-energy transitions of complexes **3–5** involve a transfer of the Pt  $d$  electrons from the top of the valence band (see the diagram in Figure 3) and the

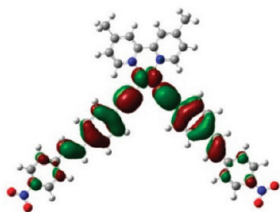
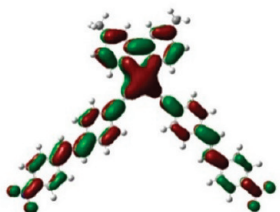
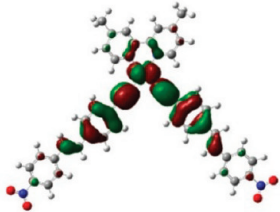
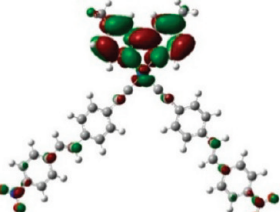
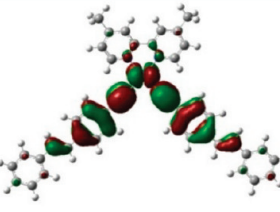
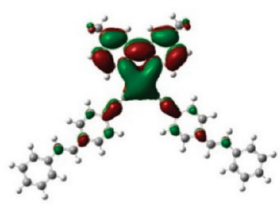
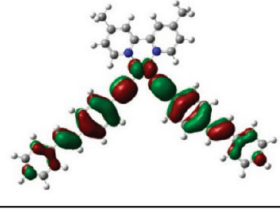
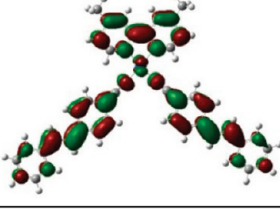
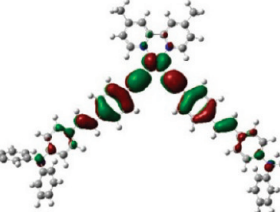
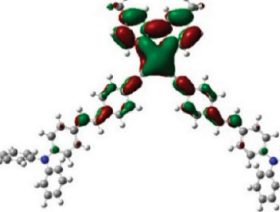
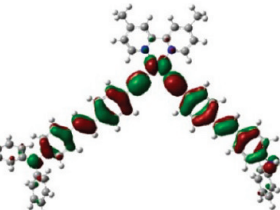
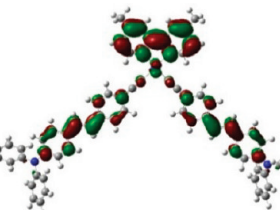
**Table 1.** Experimental and Calculated Electronic Absorption Parameters for Complexes **1–6** and Ligands **1-L**, **4-L**, **5-L**, and **6-L** in  $\text{CH}_2\text{Cl}_2$

	$\lambda_{\text{abs}}/\text{nm}$ ( $\epsilon_{\text{max}}/\text{M}^{-1} \text{cm}^{-1}$ ) <sup>a</sup>	Theor. $\lambda_{\text{abs}}/\text{nm}$ (ex. state; $f_{\text{osc}}$ ) <sup>b</sup>
<b>1</b>	401 (69330), 298 (48900)	389 (S1; 1.6529), 375 (S2; 1.8782), 353 (S3; 0.3870)
<b>2</b>	380 (90250), 292 (40080)	383 (S1; 1.4325), 367 (S2; 1.4423), 347 (S3; 1.1505)
<b>3</b>	420 (14580), 363 (78730), 349 (88280), 333 (74500)	378 (S1; 0.8110), 364 (S2; 0.9787), 333 (S3; 1.7741)
<b>4</b>	410 (16480), 360 (87300), 344 (97850), 325 (77380)	381 (S1; 0.6476), 364 (S2; 0.8692), 329 (S3; 1.7507)
<b>5</b>	415 (14980), 365 (89250), 349 (103480), 335 (87230)	384 (S1; 0.7001), 368 (S2; 0.9100), 333 (S3; 1.8807)
<b>6</b>	385 (100480), 305 (62130)	389 (S1; 1.3019), 374 (S2; 1.04375), 352 (S3; 1.5416)
<b>1-L</b>	360 (24260), 283 (9190)	
<b>4-L</b>	340 (19470), 325 (30500), 311 (26980)	
<b>5-L</b>	354 (28960, sh.), 336 (42850), 314 (30940, sh.)	
<b>6-L</b>	384 (32130), 300 (24020)	

<sup>a</sup> $\lambda_{\text{abs}}$  is the absorption wavelength, and  $\epsilon_{\text{max}}$  is molar extinction coefficient. <sup>b</sup>Theor.  $\lambda_{\text{abs}}$  is the calculated wavelength corresponding to the transition between the ground and excited states of interest (the number of the excited state is shown in parentheses), and  $f_{\text{osc}}$  is the calculated oscillator strength for the corresponding excitations.

stilbenylacetylide ligand to the bipyridine (bpy) moiety. The MLCT/LLCT characters of these transitions explain their relatively small oscillator strengths (intensities of peaks in absorption spectra). Due to unequal interaction of the ligand field with the participating Pt  $d$  orbitals of different symmetry, these excited states are noticeably separated (by  $\sim 0.5$  eV) from higher-energy states, which explains the appearance of the well-separated, low-intensity shoulder in the absorption spectra of these compounds. The second absorption band of compounds **3–5** can mainly be described as the  $\pi, \pi^*$  intraligand transition within the stilbenylacetylide ligands with an admixture of the

Table 2. NTOs<sup>a</sup> Representing Transitions That Correspond to the First and the Second Lower-Energy “Bands” for Complexes 1, 4, and 6<sup>b</sup>

Excited state number and properties	Hole	Electron
<b>1</b>		
<b>S1</b> $f_{\text{osc}} = 1.6529$ 3.19 eV (389 nm)		
<b>S3</b> $f_{\text{osc}} = 0.3870$ 3.51 eV (353 nm)		
<b>4</b>		
<b>S1</b> $f_{\text{osc}} = 0.6476$ 3.26 eV (381 nm)		
<b>S3</b> $f_{\text{osc}} = 1.7507$ 3.77 eV (329 nm)		
<b>6</b>		
<b>S1</b> $f_{\text{osc}} = 1.3019$ 3.19 eV (389 nm)		
<b>S3</b> $f_{\text{osc}} = 1.5416$ 3.53 eV (352 nm)		

<sup>a</sup>Note that excited-state NTOs differ from the ground-state MOs and rather can be considered as the linear combination of the ground-state MOs that contribute to a given excited state. The NTOs were calculated based on the optimized ground-state geometry. Each electronic transition  $S_n$  is presented as a single electron–hole pair excitation from the occupied “hole” NTO to the unoccupied “electron” NTO. <sup>b</sup>The excited-state number, corresponding oscillator strengths, and excitation energies are shown for each optical transition.

MLCT/LLCT character (see NTOs for the third excited state, S3, in Table 2). This band is more sensitive to the type of substituent and red-shifted in case of the stronger electron donor or acceptor attached to the stilbenyl moiety.

In contrast, the lowest-energy absorption bands of complexes 1, 2, and 6 are predicted to have strong contribution of the  $\pi, \pi^*$

intraligand transition, with some mixture of the MLCT and LLCT characters (see Table 2). Significant ligand  $\pi, \pi^*$  character of these transitions gives rise to the intensity of the lowest-energy absorption band of these complexes, as can be seen in Figure 1c. NTOs in Table 2 for complexes 1 and 6 illustrate the delocalized nature of the lowest-energy excited



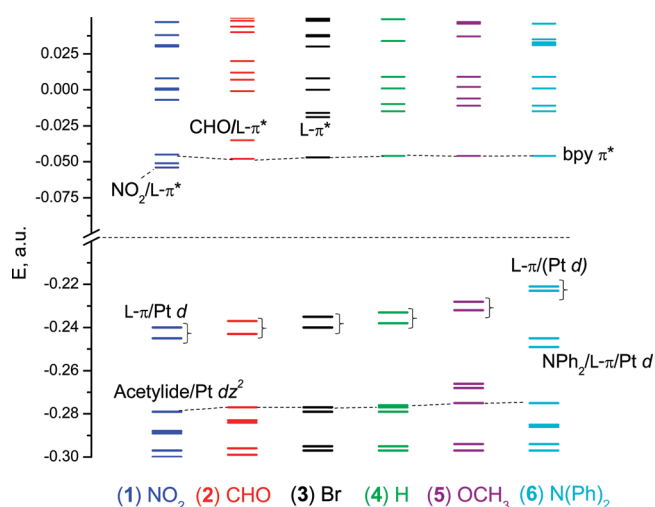


**Figure 3.** Ground-state molecular orbital energy diagram for complexes 1–6 calculated in dichloromethane using the CAM-B3LYP functional and the LANL08 basis set for the Pt atom and the 6-31G\* basis set for other atoms.

states that contribute to the absorption band, which results in larger oscillator strengths for these transitions. The higher-lying excitations can rather be characterized as the LLCT transitions from the stilbenylacetylides to the bpy moiety mixed with MLCT character, which explains their lower intensity.

In general, the shape of the absorption spectra of the discussed Pt complexes with the stilbenylacetylide ligands depends on the interplay between the states with charge-transfer character (LLCT and MLCT) and the intraligand  $\pi, \pi^*$  transitions. Thus, the complexes with the weak donor/acceptor substituents (3–5) exhibit a MLCT/LLCT shoulder in the lower-energy region of the spectra. In the cases when the stilbenylacetylides are substituted with a stronger electron-donor/acceptor substituent (1, 2, and 6), the lower-energy MLCT/LLCT states strongly mix with the intraligand  $\pi, \pi^*$  transitions, which causes larger transition dipole moments and stronger absorption intensity. The ground-state MO diagram shown in Figure 3 provides a better understanding of the effect of the substituent on energy levels and absorption spectra of the Pt complexes discussed herein. The highest occupied orbitals are delocalized over the stilbenylacetylide ligands ( $L-\pi$ ) and have noticeable Pt-d contribution, while the lowest unoccupied orbitals are predominantly delocalized over the bipyridine ligand ( $bpy-\pi^*$ ), except for complex 1. Addition of the electron-donating groups, such as  $OCH_3$  (5) and  $NPh_2$  (6), increases the ground-state dipole moment and raises the energies of the HOMOs. For complex 6, HOMO and HOMO–1 can be characterized as the pure ligand  $\pi$  ( $L-\pi$ ) orbitals with very little Pt-d admixture. Addition of electron-withdrawing substituents, such as  $NO_2$  (1) and CHO (2), lowers the energies of the unoccupied levels, which lie very close to or even below (as in complex 1) the  $bpy-\pi^*$  level. Therefore, addition of stronger electron-donor or stronger electron-acceptor groups leads to a smaller HOMO–LUMO gap (red shift in absorption spectra) and change in the character of the lowest-energy absorption bands.

Addition of polar solvents compensates for the static and the transition dipole moments induced by the strong electron-donating/accepting groups and stabilizes the donor/acceptor electronic levels. This is equivalent to shifting HOMOs to lower energies, while the LUMO localized on the stilbenyl

moves to the higher energy, resulting in blue shifts (a larger gap between levels) of the absorption bands with an increase in the solvent polarity, as shown in Figure 2. The blue shift of the absorption bands with the increased solvent polarity is observed for both the complexes with the weak electron-donor/acceptor groups (3–5) and those with strong electron-donor/acceptor groups (1, 2 and 6), while the overall shape of the absorption spectra is negligibly affected by the solvent polarity.

**Photoluminescence.** All of the complexes exhibit weak emission both at room temperature in dichloromethane solution and at 77 K in butyronitrile glassy matrix. The emission spectra of complexes 1–6 at room temperature are shown in Figure 4,

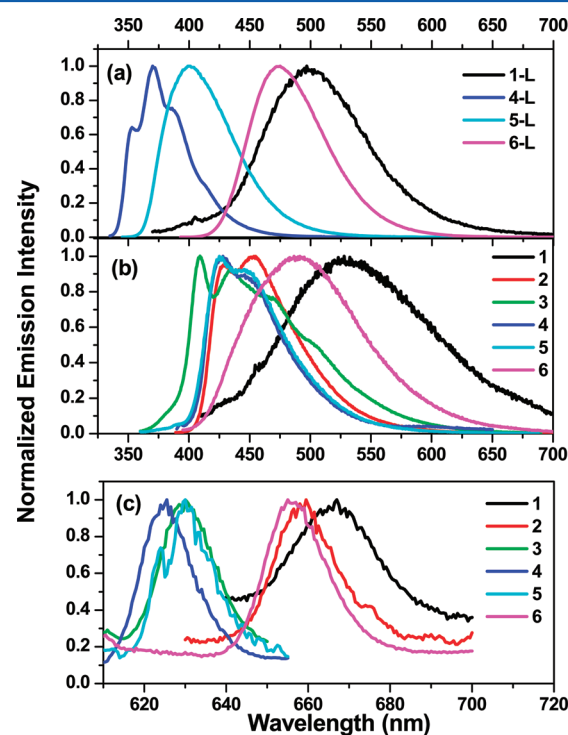


**Figure 4.** Normalized emission spectra of (a) ligands 1-L, 4-L, 5-L, and 6-L and (b) complexes 1–6 in dichloromethane at room temperature; (c) complexes 1–6 in butyronitrile glassy matrix at 77 K (phosphorescence).

and the emission data are summarized in Table 3. The emission band(s) of 2–5 at room temperature are mirror images to those of their respective major absorption band(s) with Stokes shifts smaller than 80 nm, while the emission of 1 and 6 at room temperature is broad and structureless, with Stokes shifts of 129 and 107 nm, respectively. The emission lifetimes of these complexes could not be detected by our spectrometer due to the very short lifetime ( $<5$  ns). These features suggest that the observed emission for complexes 1–6 at room temperature emanates from the singlet excited state of the stilbenylacetylide ligand. At 77 K, the emission of 1–6 appears at 625–667 nm (Figure 4c), which is assigned to the phosphorescence of the complexes. However, due to the very weak signal, the phosphorescence lifetimes have not been determined.

In previous studies<sup>17</sup> of compound 4, the singlet  $^1\pi, \pi^*$  state has been proposed to relax predominantly through the intersystem crossing into the triplet  $^3\pi, \pi^*$  state, which explains the observed relatively weak fluorescence. The triplet  $^3MLCT$  emission has also been observed in a similar series of complexes but shown to undergo a quick nonradiative decay through the

**Table 3.** Photoluminescence and Excited-State Absorption Parameters for Complexes 1–6 and Ligands 1-L, 4-L, 5-L, and 6-L

	$\lambda_{\text{em}}/\text{nm}$ ( $\Phi_{\text{em}}$ ) <sup>a</sup>	RT 77 K	$\lambda_{\text{T}_1-\text{T}_n}/\text{nm}$ ( $\tau_{\text{T}}/\text{ns}$ ; $\epsilon_{\text{T}_1-\text{T}_n}/\text{M}^{-1}\text{cm}^{-1}$ ; $\Phi_{\text{T}}$ ) <sup>c</sup>	$\lambda_{\text{S}_1-\text{S}_n}/\text{nm}$ ( $\tau_{\text{S}}/\text{ps}$ ) <sup>d</sup>	Theor $\lambda_{\text{fluo}}$ /nm	Theor $\lambda_{\text{phos}}$ /nm
1	530 (0.012)	667	480 (385; 67825; –), 750 (401; 98760; 0.17)	495 (59), 580 (58)	497	663
2	454 (0.008)	659	510 (225; 184760; 0.079)	532 (77), 626 (74)	472	–
3	409 (0.017)	630	435 (48; –; –)	465 (14)	449	638
4	425 (–)	625	460 (64; –; –)	460 (69)	452	638
5	428 (0.009)	630	460 (73; –; –)	468 (205)	460	–
6	492 (0.003)	656	520 (198; 235510; 0.075)	526 (18)	463	668
1-L	499 (0.007)	–	435 (–), 602 (–)	467 (91), 562 (121)	–	–
4-L	370 (0.10)	–	505 (–)	606 (43)	–	–
5-L	401 (0.03)	–	510 (–)	550 (22)	–	–
6-L	474 (0.58)	–	470 (–)	444 (95), 602 (59)	–	–

<sup>a</sup>In CH<sub>2</sub>Cl<sub>2</sub>. <sup>b</sup>In BuCN glassy matrix. <sup>c</sup>Triplet excited-state absorption band maximum ( $\lambda_{\text{T}_1-\text{T}_n}$ ), molar extinction coefficient ( $\epsilon_{\text{T}_1-\text{T}_n}$ ), quantum yield ( $\Phi_{\text{T}}$ ), and lifetime ( $\tau_{\text{T}}$ ) measured in CH<sub>3</sub>CN/CH<sub>2</sub>Cl<sub>2</sub> solution (v/v = 10:1). <sup>d</sup>Singlet excited-state absorption band maximum ( $\lambda_{\text{S}_1-\text{S}_n}$ ) and lifetime ( $\tau_{\text{S}}$ ) measured in CH<sub>3</sub>CN/CH<sub>2</sub>Cl<sub>2</sub> solution.

relaxation of the stilbene ligand(s) into the cis conformation.<sup>17</sup> The energy levels of the  $^3\pi,\pi^*$  states relative to the  $^3\text{MLCT}$  states have been shown to strongly depend on the type of substituent on the 4,4'-position of the bpy ligand because of a strong influence of the substituent on the  $^3\text{MLCT}$  energies.<sup>41</sup> Similar to previous studies, we found a strong effect on the relative positioning between the  $^3\pi,\pi^*$  and  $^3\text{MLCT}$  states that is caused by the strength of the electron-donor/acceptor substituent on the stilbene.

To elucidate the nature of emission of complexes 1–6, their spectra are compared to the emission of the corresponding ligands 1-L, 4-L, 5-L, and 6-L (Figure 4a). The emission of 4-L can be assigned to the  $^1\pi,\pi^*$  transition by comparing to the *trans*-stilbene emission reported in the literature.<sup>42</sup> The  $^1\pi,\pi^*$  character of the singlet emission in this ligand is also well presented in the NTOs, as shown in Figure 5. Compound 5-L emits at a similar level as 4-L (therefore, its NTOs are not shown in Figure 5), while the 1-L and 6-L spectra are significantly red-shifted due to the presence of strong electron-accepting/donating groups. NTOs for the relaxed singlet excited-state geometries, corresponding to the fluorescence, show that strong electron-donating substituent NPh<sub>2</sub> delocalizes the hole NTO over both the stilbene and the substituent group, while showing more localized character of the electron NTO on the stilbene with insignificant electron density on the substituent group (see the bottom panel in Figure 5). The strong electron-withdrawing NO<sub>2</sub> group has an opposite effect, with the more delocalized character of the electron NTO than the hole. Such a difference in delocalization between the electron and hole NTOs explains the red shift in the fluorescence of ligands 1-L and 6-L compared to that of other ligands.

The emission spectra of complexes 1 and 6 very closely represent emission of their ligands, with a slight red shift, which is indicative of the predominant intraligand character of the photoluminescence in this range (see Figure 4). However, the

width of the spectra significantly increases as a result of some interactions with Pt d orbitals, as well as strong electron–vibrational couplings. The other complexes emit at substantially lower energy compared to their corresponding ligands, which suggests a strong delocalization induced by platinum d $\pi$  orbitals, and significant contribution from  $^1\text{MLCT}/^1\text{LLCT}$ , as discussed in the following paragraph.

Overall, TD-DFT calculations of the singlet and triplet emission reproduce the trends observed experimentally, as summarized in Table 3. NTOs for the relaxed singlet and triplet excited-state geometries (corresponding to fluorescence and phosphorescence, respectively) are illustrated in Figure 5 and compared with the NTOs contributing to the singlet emission of the corresponding stilbenylacetylide ligands. The singlet emission of complex 1 stems from the intraligand  $^1\pi,\pi^*$  transition in one of the single stilbenylacetylide ligands, which becomes slightly twisted relative to the Pt coordination plane and, thus, hinders the  $^1\text{MLCT}$  character of fluorescence in this compound. Interestingly, the character of the NTOs contributing to singlet emission of this compound has a very different nature compared to that of NTOs contributing to the lowest-energy absorption (compare NTOs in Figure 5 with S1 in Table 2 for 1). Such a significant difference in NTOs is a sign of a strong exciton–vibration coupling, which is evident by a broadening of the fluorescence peak of complex 1 compared to that of 1-L shown in Figure 4. In all other complexes, NTOs contributing to fluorescence are strongly mixed with the  $^1\text{MLCT}$  from Pt to the bpy moiety, as well as LLCT between the stilbene and bpy. Strong charge-transfer character of the NTOs involved in the singlet emission explains the experimentally observed red shift in the emission maxima of these complexes versus the fluorescence energies of their ligands.

Triplet-state emission for compounds 1 and 6 involves a symmetric  $^3\pi,\pi^*$  transition in both stilbenylacetylide ligands (Figure 5, right panel), while phosphorescence of complexes with the weaker donor/acceptor substituents predominantly carries the  $^3\text{LLCT}/^3\text{MLCT}$  character. The red shift of the photoluminescence spectra observed for complexes with the stronger electron-accepting/donating groups (1 and 6) can be explained by the interplay between the  $^3\pi,\pi^*$  electronic levels of the stilbenylacetylide ligands and the  $^3\text{MLCT}/^3\text{LLCT}$  states, similar to the picture discussed in the absorption section. Strong electron-donating/accepting groups lower the energies of the stilbene  $^3\pi,\pi^*$  transitions relative to those of the  $^3\text{MLCT}/^3\text{LLCT}$  states, so that the lowest excited states bear more of the  $^3\pi,\pi^*$  character. This process is highly sensitive to the solvent polarity as the polar solvent can partially stabilize the dipole moment induced by the substituent group and raise the intraligand transition energies. In other words, in a less polar solvent,  $^3\pi,\pi^*$  transitions have more admixture of  $^3\text{MLCT}/^3\text{LLCT}$  character.

Combining all of the evidence discussed above, the emission parentage of the complexes is assigned as follows: the emission of complexes 1 and 6 is dominated by the ligand-centered  $\pi,\pi^*$  transition localized on the stilbenylacetylide ligands, but complex 6 has some admixture of the  $^1\text{MLCT}/^1\text{LLCT}$  characters in its fluorescence. The emission of complexes 2–5 can be characterized by the mixture of major MLCT/LLCT and little intraligand  $\pi,\pi^*$  transitions. The short-lived and weak fluorescence of the complexes at room temperature can be accounted for by existence of the twisted geometry of the ligands, which may serve as a nonradiative decay pathway of the



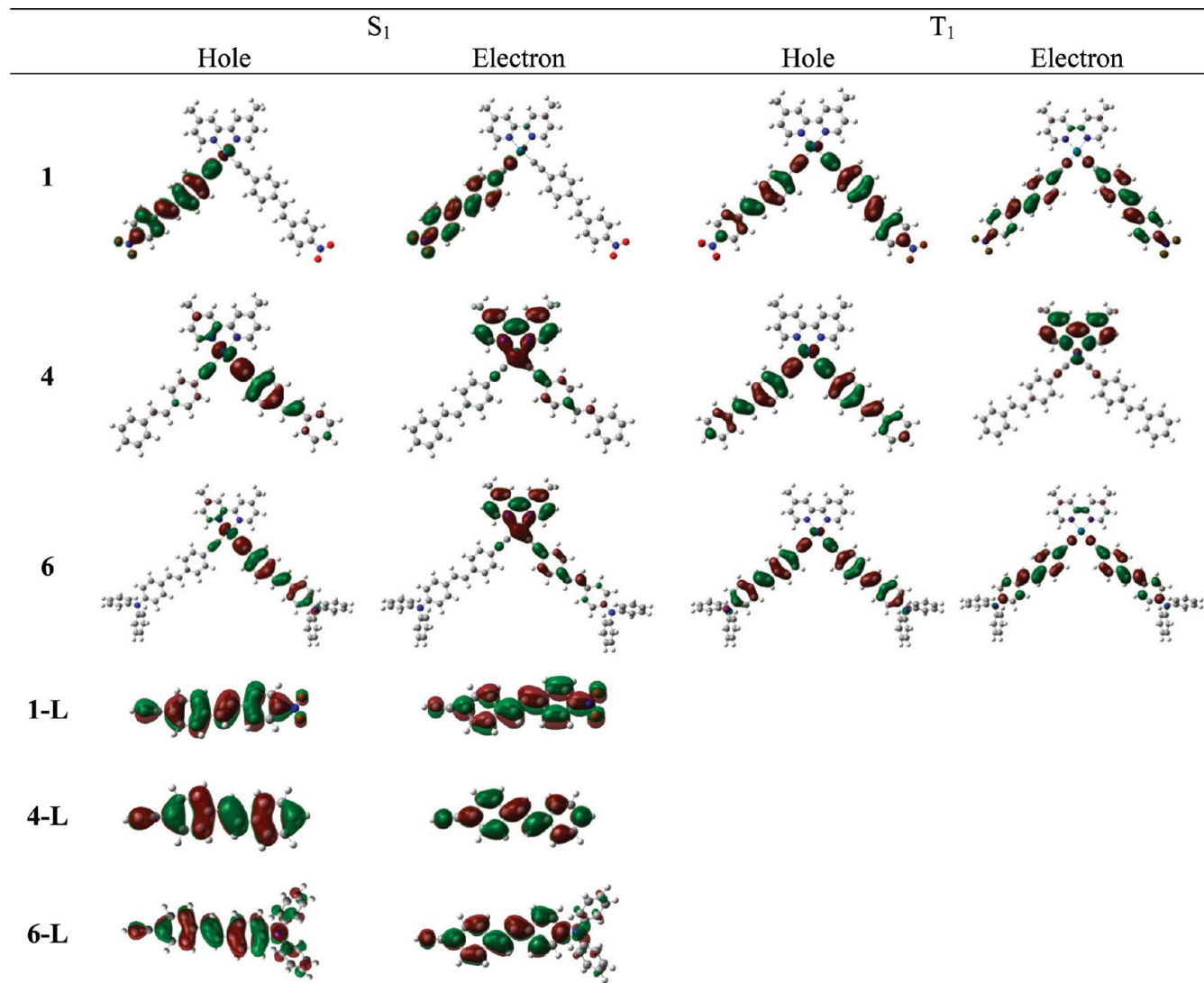


**Figure 5.** NTO plots for the singlet ( $S_1$ ) and triplet ( $T_1$ ) emissions (corresponding to the fluorescence and phosphorescence, respectively) for complexes **1**, **4**, and **6** and their corresponding ligands **1-L**, **4-L**, and **6-L**. NTOs were obtained based on the optimized excited-state geometry to simulate the photoluminescence.

excited state.<sup>17</sup> Overall, variation of the substituent at the 4'-position of the stilbenylacetylide ligands has a significant influence on the emission energy and electronic state of the complexes.

**Transient Absorption.** The nanosecond and femtosecond transient absorption (TA) measurements for complexes **1–6** and ligands **1-L**, **4-L**, **5-L**, and **6-L** were carried out. From the TA experiment, we can obtain the spectral features and lifetimes of the singlet and triplet excited states. The spectral region where the excited-state absorption is stronger than the ground-state absorption can be identified from the positive absorption band(s) of the TA spectrum, while the excited-state lifetime can be deduced from the decay of the TA and the triplet excited-state quantum yield is determined by the relative actinometry.

The nanosecond TA spectra of complexes **1–6** in a  $\text{CH}_3\text{CN}/\text{CH}_2\text{Cl}_2$  ( $v/v = 10/1$ ) solution at zero delay after excitation are shown in Figure 6. All of the complexes exhibit strong TA signals that are well time-resolved, as illustrated by the time-resolved spectra of **1–6** in Supporting Information Figures S2–S7. The TAs of the complexes are significantly enhanced

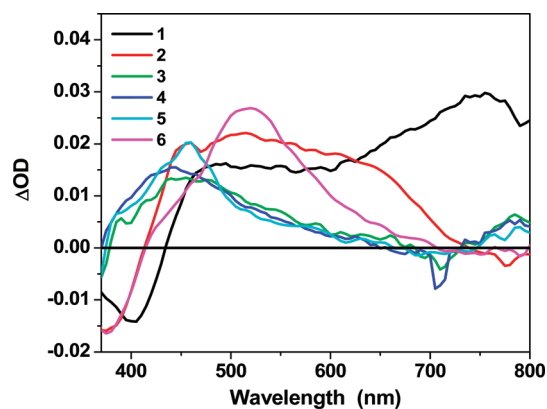


**Figure 6.** Nanosecond transient difference absorption spectra of complexes **1–6** in  $\text{CH}_3\text{CN}/\text{CH}_2\text{Cl}_2$  ( $v/v = 10/1$ ) immediately after 4.1 ns laser excitation.  $\lambda_{\text{ex}} = 355$  nm, and  $A_{355} = 0.4$  in a 1 cm cuvette.

compared to those of their corresponding ligands (Figure S1 in the Supporting Information), indicating enhanced intersystem crossing (ISC) induced by the heavy-atom effect of Pt.

Complexes **1** and **2** that bear strong electron-withdrawing substituents show especially broad and strong transient absorptions, while the shapes of the TA spectra of the other complexes resemble those of their corresponding ligands. For all complexes, a bleaching band was observed at  $\lambda < 450$  nm, which is consistent with the position of the major absorption band in their UV–vis absorption spectra. The triplet lifetime deduced from the decay of the TA and the molar extinction coefficient of the triplet excited-state absorption determined from the singlet depletion method<sup>37</sup> for **1**, **2**, and **6** are listed in Table 2. Similar to those trends observed from the UV–vis absorption and emission spectra, the bleaching band and TA absorption band are red-shifted for complexes **1**, **2**, and **6** in comparison to those of **3**–**5**. The triplet excited-state lifetimes of **1**, **2**, and **6** are also significantly longer than those of **3**–**5**, which indicates different natures of the excited state that gives rise to the TA. For complex **4**, the feature of the TA spectrum and the lifetime are quite similar to those reported by Schanze and co-workers for a similar Pt(II) bipyridyl bis-(ethynylstilbene) complex, in which the transient is believed to be a stilbene-localized  $^3\pi,\pi^*$  state with the double bond in the trans geometry.<sup>17</sup> The short lifetime should be attributed to the rapid nonradiative decay induced by the C=C bond rotation in the stilbene moiety. The similar TA patterns for **3** and **5** to those of their respective ligands and to **4** imply that the excited state that gives rise to the TA is the stilbene-localized  $^3\pi,\pi^*$  state as well.

For complexes **1** and **2**, the TA spectra are much broader, and a strong new absorption band appears at 750 nm for **1**. With reference to the TA study reported by Castellano and co-workers for Pt terpyridyl acetylide complexes bearing  $\pi$ -conjugated arylacetylides,<sup>43</sup> the near-IR TA band of **1** could possibly originate from the acetylide cation generated from the LLCT/ILCT (intraligand charge-transfer from the stilbene to the nitro group) processes. Therefore, the excited state that gives rise to the observed TA for **1** is tentatively assigned to the stilbene-localized  $^3\pi,\pi^*$  state, mixed with LLCT/ILCT characters. We believe that the TA for **2** has a similar origin.

The femtosecond time-resolved TA spectra of **1**–**6** in a mixed CH<sub>3</sub>CN/CH<sub>2</sub>Cl<sub>2</sub> solution are shown in Figure 7 and in

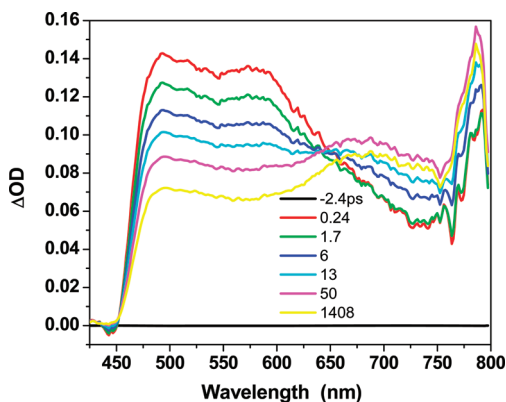


**Figure 7.** Femtosecond time-resolved transient difference absorption spectrum of complex **1** in CH<sub>3</sub>CN/CH<sub>2</sub>Cl<sub>2</sub> (v/v = 10/1).  $\lambda_{\text{ex}}$  = 400 nm.

the Supporting Information. The TA spectra of **2**–**5** resemble those of their nanosecond TA spectra and thus are assigned to the same transients as those contributing to the nanosecond TA, which could be from the singlet excited state or the triplet excited state in case the intersystem crossing is very fast.

Complex **1** exhibits a different time-resolved pattern. As shown in Figure 7, at a 0.24 ps delay after laser excitation, two broad bands at 493 and 577 nm and a narrow band at 785 nm appear, which are similar to those observed in its nitrostilbenylethyne ligand (see Supporting Information Figure S12). The intensities of the 493 and 577 nm bands are gradually reduced, while the 785 nm band increases and a new broad band at 683 nm emerges. An isosbestic point is observed at 647 nm. At a 50 ps delay, the intensities of the bands at 683 and 785 nm reach the maxima, and the full spectrum resembles that of the nanosecond TA. These characteristics suggest the intersystem crossing from the singlet to the triplet excited state completed within 50 ps. At a longer delay time, the TA spectrum slowly decays, reflecting the longer lifetime of the triplet excited state. The singlet TA band maxima and the lifetimes of the singlet excited states deduced from the decay of the femtosecond TAs for **1**–**6** are listed in Table 3.

**Reverse Saturable Absorption.** As discussed above, both the nanosecond and femtosecond TA spectra of **1**–**6** exhibit positive absorption at 532 nm, indicating a stronger excited-state absorption than that of the ground state. In addition, the triplet excited-state lifetime is longer than the nanosecond laser pulse width (4.1 ns). Therefore, it is expected that reverse saturable absorption (RSA), defined as a decreased transmission upon increase of incident fluence, would occur for a nanosecond laser pulse at 532 nm. To demonstrate this, a nonlinear transmission experiment using complexes **1**–**6** at 532 nm for nanosecond laser pulses was carried out in dichloromethane solution at a linear transmittance of 80% in a 2 mm cuvette. The results are shown in Figure 8. The transmission of the

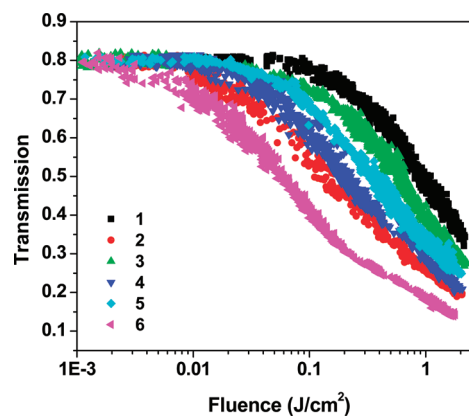


**Figure 8.** Nonlinear transmission curves of **1**–**6** in CH<sub>2</sub>Cl<sub>2</sub> solution for 4.1 ns laser pulses at 532 nm. The path length of the cuvette is 2 mm, and the linear transmission of the solution is adjusted to 80% at 532 nm in the 2 mm cuvette.

complexes drastically decreases with increased incident fluence, clearly demonstrating a strong RSA. The degree of RSA of the complexes increases in the order of  $1 < 3 < 5 < 4 < 2 < 6$ . The degree of RSA for **6** is even stronger than that of the 2,2'-bipyridine Pt(II) complex bearing a 2-(benzothiazol-2'-yl)-9,9-diethyl-7-ethynylfluorene complex reported by our group earlier.<sup>11</sup> The stronger RSAs of **2** and **6** can be accounted for by their much stronger excited-state absorption (both singlet and triplet) at 532 nm relative to that of other complexes, which is clearly evident from the nanosecond and femtosecond TA spectra. To quantitatively explain the RSA trend, nanosecond and picosecond Z-scan experiments should be conducted and the data fitted via a five-level model to extract the excited-state

absorption cross sections and deduce the ratios of the excited-state absorption cross sections relative to those of the ground state. This work is currently in progress.

## CONCLUSION

A series of platinum bipyridyl platinum(II) bisstilbenylacetylide complexes with different auxiliary substituents on the stilbenylacetylide ligands were synthesized, and the photophysics of these complexes were systematically characterized by spectroscopic measurements and TD-DFT theoretical calculations. The absorption and emission characteristics of these complexes can be substantially adjusted by the auxiliary ligands. While the substitution of H on the 4'-position of stilbene by Br and OMe groups does not alter the photophysical properties of the complexes eminently, the absorption and the emission characteristics are significantly tuned by the CHO, NO<sub>2</sub>, and NPh<sub>2</sub> substituents. The lowest-energy absorption bands of 3–5 are dominated by the MLCT/LLCT transitions with an admixture of the  $\pi, \pi^*$  character, while the lowest absorption bands for complexes 1, 2, and 6 are dominated by the ligand-centered  $\pi, \pi^*$  transition with the admixture of MLCT/LLCT characters (in strong dependence of the solvent polarity). Emission shows very similar trends. The nanosecond and femtosecond transient difference absorptions of the complexes feature strong absorption in the visible spectral region, which can be attributed to a stilbene-localized  $\pi, \pi^*$  state with the double bond in the trans geometry. The TA spectra of complexes 1 and 2 that bear strong electron-withdrawing substituents are very broad and extend to the near-IR region, suggesting contribution from the acetylide ligand cation that results from the LLCT/ILCT transitions. All complexes exhibit strong reverse saturable absorption for the nanosecond laser pulse at 532 nm, with complex 6 showing the strongest RSA due to the very strong excited-state absorption relative to that of the ground state at 532 nm. This makes complex 6 a very promising candidate for devices that require strong RSA.

## ASSOCIATED CONTENT

### Supporting Information

The synthetic procedures and characterization data for 11, 12, 3-L, and 1–6, characterization data for 21 and 22, optimized molecular structures for 1–6 via DFT calculations, ground-state molecular orbitals for 1, 4, and 6, NTO plots for the lowest excited states of 1–6 calculated in CH<sub>2</sub>Cl<sub>2</sub>, NTO plots for the lowest excited states 1 and 4 calculated in toluene, nanosecond TA spectra of ligands 1-L and 4-L–6-L at zero time delay, nanosecond time-resolved TA spectra of 1–6, femtosecond time-resolved TA spectra of 2-6, 1-L, and 2-L–6-L, and the full ref 24. This material is available free of charge via the Internet at <http://pubs.acs.org>.

## AUTHOR INFORMATION

### Corresponding Author

\*Phone: 701-231-6254. E-mail: Wenfang.Sun@ndsu.edu.

### Notes

The authors declare no competing financial interest.

## ACKNOWLEDGMENTS

This work is supported partially by National Science Foundation (CAREER CHE-0449598) and partially by the Army Research Laboratory (W911NF-06-2-0032 and W911NF-10-2-0055) to

W.S. S.K. acknowledges financial support from ND NSF EPSCoR Grant (EPS-0814442).

## REFERENCES

- (1) (a) Lu, W.; Mi, B.-X.; Chan, C.-W.; Hui, Z.; Che, C.-M.; Zhu, N.; Lee, S.-T. *J. Am. Chem. Soc.* **2004**, *126*, 4958. (b) He, Z.; Wong, W.-Y.; Yu, X.; Kwok, H.-S.; Lin, Z. *Inorg. Chem.* **2006**, *45*, 10922.
- (2) Du, P.; Eisenberg, R. *Chem. Sci.* **2010**, *1*, 502.
- (3) Wu, W.; Xu, X.; Yang, H.; Hua, J.; Zhang, X.; Zhang, L.; Long, Y.; Tian, H. *J. Mater. Chem.* **2011**, *21*, 10666.
- (4) Keck, M. V.; Lippard, S. J. *J. Am. Chem. Soc.* **1992**, *114*, 3386.
- (5) Lottner, C.; Knuechel, R.; Bernhardt, G.; Brunner, H. *Cancer Lett.* **2004**, *203*, 171.
- (6) Chan, C.-W.; Cheng, L.-K.; Che, C.-M. *Coord. Chem. Rev.* **1994**, *132*, 87.
- (7) Miskowski, V. M.; Houlding, V. H.; Che, C.-M.; Wang, Y. *Inorg. Chem.* **1993**, *32*, 2518.
- (8) Hissler, M.; Connick, W. B.; Geiger, D. K.; McGarrah, J. E.; Lipa, D.; Lachicotte, R. J.; Eisenberg, R. *Inorg. Chem.* **2000**, *39*, 447.
- (9) Whittle, C. E.; Weinstein, J. A.; George, M. W.; Schanze, K. S. *Inorg. Chem.* **2001**, *40*, 4053.
- (10) (a) Castellano, F. N.; Pomestchenko, I. E.; Shikhova, E.; Hua, F.; Muro, M. L.; Rajapakse, N. *Coord. Chem. Rev.* **2006**, *250*, 1819. (b) Pomestchenko, I. E.; Luman, C. R.; Hissler, M.; Ziesler, R.; Castellano, F. N. *Inorg. Chem.* **2003**, *42*, 1394.
- (11) Sun, W.; Zhang, B.; Li, Y.; Pritchett, T. M.; Li, Z.; Haley, J. E. *Chem. Mater.* **2010**, *22*, 6384.
- (12) Chan, S.-C.; Chan, M. C. W.; Wang, Y.; Che, C.-M.; Cheung, K.-K.; Zhu, N. *Chem.—Eur. J.* **2001**, *7*, 4180.
- (13) (a) Hissler, M.; McGarrah, J. E.; Connick, W. B.; Geiger, D. K.; Cummings, S. D.; Eisenberg, R. *Coord. Chem. Rev.* **2000**, *208*, 115. (b) McGarrah, J. E.; Kim, Y.-J.; Hissler, M.; Eisenberg, R. *Inorg. Chem.* **2001**, *40*, 4510.
- (14) Lu, W.; Chan, M. C. W.; Zhu, N.; Che, C.-M.; He, Z.; Wong, K. Y. *Chem.—Eur. J.* **2003**, *9*, 6155.
- (15) He, G. S.; Tan, L.-S.; Zheng, Q.; Prasad, P. N. *Chem. Rev.* **2008**, *108*, 1245.
- (16) (a) Svetlichnyi, V. A.; Meshalkin, Y. P. *Opt. Commun.* **2007**, *280*, 379. (b) Huang, Z.; Wang, X.; Li, B.; Lv, C.; Xu, J.; Jiang, W.; Tao, X.; Qian, S.; Chui, Y.; Yang, P. *Opt. Mater.* **2007**, *29*, 1084. (c) Zhou, X.; Ren, A.-M.; Feng, J.-K.; Liu, X.-J. *Chem. Phys. Lett.* **2002**, *362*, 541.
- (17) Haskins-Glusac, K.; Ghiviriga, I.; Abboud, K. A.; Schanze, K. S. *J. Phys. Chem. B* **2004**, *108*, 4969.
- (18) Domínguez-Gutiérrez, D.; De Paoli, G.; Guerrero-Martínez, A.; Ginocchietti, G.; Ebeling, D.; Eiser, E.; De Cola, L.; Elsevier, C. J. *J. Mater. Chem.* **2008**, *18*, 2762.
- (19) Heck, R. F.; Nolley, J. P. *J. Org. Chem.* **1972**, *37*, 2320.
- (20) Reinhard, W. H. *Angew. Chem., Int. Ed.* **2001**, *40*, 1411.
- (21) Hassan, J.; Sévignon, M.; Gozzi, C.; Schulz, E.; Lemaire, M. *Chem. Rev.* **2002**, *102*, 1359.
- (22) Sonogashira, K.; Tohda, Y.; Hagihara, N. *Tetrahedron Lett.* **1975**, *16*, 4467.
- (23) (a) Hockless, D. C. R.; Whittall, I. R.; Humphrey, M. G. *Acta Crystallogr., Sect. C* **1996**, *52*, 3222. (b) Rodri, J. G.; Lafuente, G. A.; Arranz, J. J. *Polym. Sci., Part A: Polym. Chem.* **2005**, *43*, 6438. (c) Zhao, H.; Yuan, W. Z.; Tang, L.; Sun, J. Z.; Xu, H.; Qin, A.; Mao, Y.; Jin, J. K.; Tang, B. Z. *Macromolecules* **2008**, *41*, 8566. (d) Rigamonti, L.; Babgi, B.; Cifuentes, M. P.; Roberts, R. L.; Petrie, S.; Stranger, R.; Righetto, S.; Teshome, A.; Asselberghs, I.; Clays, K.; Humphrey, M. G. *Inorg. Chem.* **2009**, *48*, 3562.
- (24) Frisch, M. J.; et al. *Gaussian 09*, revision A.1; Gaussian, Inc.: Wallingford, CT, 2009.
- (25) Yanai, T.; Tew, D.; Handy, N. *Chem. Phys. Lett.* **2004**, *393*, 51.
- (26) (a) Roy, L. E.; Scalmani, G.; Kobayashi, R.; Batista, E. R. *Dalton Trans.* **2009**, 6719. (b) Peach, M. J. G.; Benfield, P.; Helgaker, T.; Tozer, D. J. *J. Chem. Phys.* **2008**, *128*, 044118. (c) Vlček, A., Jr.; Zális, S. *Coord. Chem. Rev.* **2007**, *251*, 258.



- (27) (a) Barone, V.; Cossi, M.; Tomasi, J. *J. Comput. Chem.* **1998**, *19*, 404. (b) Cossi, M.; Rega, N.; Scalmani, G.; Barone, V. *J. Comput. Chem.* **2003**, *24*, 669.
- (28) (a) Batista, E. R.; Martin, R. L. *J. Phys. Chem. A* **2005**, *109*, 3128. (b) Fantacci, S.; De Angelis, F.; Selloni, A. *J. Am. Chem. Soc.* **2003**, *125*, 4381. (c) Filippo, D. A.; Simona, F.; Annabella, S. *Chem. Phys. Lett.* **2004**, *389*, 204.
- (29) Furche, F.; Ahlrichs, R. *J. Chem. Phys.* **2002**, *117*, 7433.
- (30) Scalmani, G.; Frisch, M. J.; Mennucci, B.; Tomasi, J.; Cammi, R.; Barone, V. *J. Chem. Phys.* **2006**, *124*, 094107.
- (31) Martin, R. L. *J. Chem. Phys.* **2003**, *118*, 4775.
- (32) Dennington, R., II; Keith, T.; Millam, J. *GaussView*, version 4.1; Semichem Inc.: Shawnee Mission, KS, 2007.
- (33) Demas, J. N.; Crosby, G. A. *J. Phys. Chem.* **1971**, *75*, 991.
- (34) Eaton, D. F. *Pure Appl. Chem.* **1988**, *60* (7), 1107.
- (35) Li, G.; Glusac, K. D. *J. Phys. Chem. A* **2008**, *112*, 4573.
- (36) Yamaguchi, S.; Hamaguchi, H. O. *Appl. Spectrosc.* **1995**, *49*, 1513.
- (37) Carmichael, I.; Hug, G. L. *J. Phys. Chem. Ref. Data* **1986**, *15*, 1.
- (38) Firey, P. A.; Ford, W. E.; Sounik, J. R.; Kenney, M. E.; Rodgers, M. A. *J. Am. Chem. Soc.* **1988**, *110*, 7626.
- (39) Guo, F.; Sun, W.; Liu, Y.; Schanze, K. S. *Inorg. Chem.* **2005**, *44*, 4055.
- (40) (a) Badaeva, E. A.; Timofeeva, T. V.; Masunov, A.; Tretiak, S. *J. Phys. Chem. A* **2005**, *109*, 7276. (b) Meyers, F.; Bredas, J. L. *Synth. Met.* **1992**, *49*, 181.
- (41) (a) Hissler, M.; Connick, W. B.; Geiger, D. K.; McGarrah, J. E.; Lipa, D.; Lachicotte, R. J.; Eisenberg, R. *Inorg. Chem.* **2000**, *39*, 447. (b) Wadas, T. J.; Lachicotte, R. J.; Eisenberg, R. *Inorg. Chem.* **2003**, *42*, 3772. (c) Whittle, C. E.; Weinstein, J. A.; George, M. W.; Schanze, K. S. *Inorg. Chem.* **2001**, *40*, 4053.
- (42) Waldeck, D. H. *Chem. Rev.* **1991**, *91*, 415.
- (43) Wang, X.; Goeb, S.; Ji, Z.; Castellano, F. N. *J. Phys. Chem. B* **2010**, *114*, 14440.